UNIVERSITY OF CALIFORNIA
RIVERSIDE

Thermal Management of Solar Cells

A Thesis submitted in partial satisfaction
of the requirements for the degree of

Master of Science

in

Electrical Engineering

by

Mohammed Ahmed Saadah

June 2013

Thesis Committee:
Dr. Alexander A. Balandin, Chairperson
Dr. Roger Lake
Dr. Alexander Khitun

The Thesis of Mohammed Ahmed Saadah is approved by:

Committee Chairperson

University of California, Riverside

Acknowledgments

First, I wish to express my sincere appreciation to my advisor, Dr. Alexander Balandin for giving me the honor of working under his supervision, and for lending valuable support in the course of my study and research. I also wish to thank my colleagues for their continuous help and support. Finally, I wish to thank my parents and my wife for their patience and support through my years of studies.

Table of Contents

List of Figures

List of Tables

Chapter 1

Introduction

1.1 Motivation

The focus on solar cells as a source of photovoltaic energy is rapidly increasing nowadays [1]. The amount of sun's energy entering earth surface in one hour is more than the world consume in one year. The photovoltaic market has been increasing by more than 20% annually since 2002. Improving solar cells aims at increasing the power conversion efficiency and reducing manufacturing costs. Crystalline silicon is the most commonly used material in making solar cells with more than 90% market use. Solar cells manufactured in 2011 are capable or converting about 15% of its absorbed light energy into output electricity. Solar cells panels that employ optical concentrators can convert up to 30% of absorbed light into electricity. The remaining 70% of absorbed energy is turned into heat inside the solar cell. The continuous decrease in solar cells size coupled with the

increase in their energy absorption generates more heat inside the solar cells and raise their temperature. The increasing the solar cell temperature negatively affect its power conversion efficiency and can damage it. Therefore, it is important to control the solar cell temperature and effectively remove the unwanted heat. Most solar cells utilize passive cooling technologies. A basic heat sink can reduce the solar cell temperature by about 15°C, which increases the output power by 6% [2]. When a heat sink is attached to a solar cell, a thermal resistance between the two interfaces can limit the amount of heat transferred between the solar cell and heat sink. This resistance is a result of the small air gaps in between the joined surfaces and caused by the surfaces imperfections. Since air is a poor thermal conductor, we need to fill these gaps with a material that has better thermal conductivity. Thermal interface materials (TIMs) do this task and improves the interfacial contact by decreasing the thermal resistance. The goal of this research is to achieve a better thermal management of solar cells by improving the interface contact between the solar cell and a passively cooled heat sink.

1.2 Operation of Photovoltaic Solar Cell

A photovoltaic cell is a semiconductor that converts sunlight into electric power through the photovoltaic effect. This phenomenon was first discovered by Becquerel in 1839 [3]. A typical solar cell is made of a p-n junction. This junction is formed by joining n-type material with a p-type material. At equilibrium, the junction has a bandgap energy E_g that is equal to the difference between the lower edge of the conduction band and the upper edge of the valence band. Solar radiation enters the p-n junction as a beam of photons

with energy$E = hv$. If this energy equals to or more than the semiconductor's bandgap E_g, the photon is absorbed by the cell and an electron-hole pair is generated. This process of creating free electrons and holes carriers is referred to as photogeneration. The built in potential of the p-n junction causes the generated electrons to drift to the n-type region towards the external contact. Similarly, the generated holes move to the p-type region towards the p-side external contact. When electrons and holes accumulate at their prospective external contacts, a potential difference appears between the two external metal contacts and current can flow if they're connected to an external load [4].

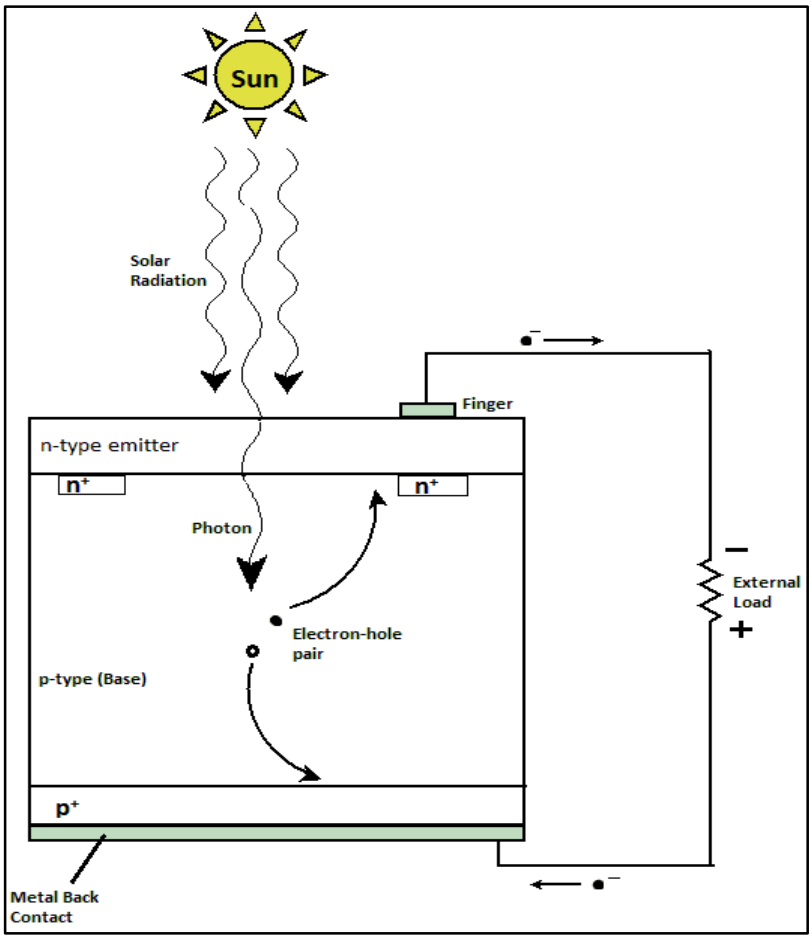

Figure 1.1 Schematic of a solar cell

Open circuit voltage V_{OC} is the voltage between the two metal terminals of an illuminated photovoltaic cell with no load connected to them and current is zero. The short-circuit current I_{sc} is obtained by connecting the two terminals together making the voltage zero. The short-circuit current would then determine the rate of photogenerated electron-hole pairs[1].

When connecting a resistive load, the current will be less than the short-circuit current I_{sc}. The voltage will also be less than the open-circuit voltage V_{OC}. The cell output power is given by:

$$P = IV$$

Where the following conditions are always valid:

$$I < I_{SC} \quad \text{and} \quad V < V_{OC}$$

To obtain the maximum power conditions we derive the diode equation above and equate it to zero:

$$dP = d(IV) = IdV + VdI = 0$$

And we get the maximum power output at:

$$P_{mp} = I_{mp}V_{mp}$$

The fill factor of a solar cell *FF* is a parameter used to evaluate the quality of the current-voltage curve, it is given by[5]:

$$FF = \frac{P_{mp}}{I_{sc}V_{oc}} = \frac{I_{mp}V_{mp}}{I_{sc}V_{oc}}$$

Which has typical value of 0.8 to 0.9 for an efficient solar cell.

The solar cell's power conversion efficiency, η is the ratio of the solar cell output power to the incident light power entering the cell.

$$\eta = \frac{P_{mp}}{P_{in}} = \frac{FF.I_{sc}V_{oc}}{P_{in}}$$

1.3 Effects of Temperature on Efficiency

Photons incident on a solar cell have different wavelengths. Photons with long wavelength will penetrate into the p-type region and photons with shorter wavelength are mostly absorbed in the n-type region. Photons with energy below the solar cell's bandgap energy E_g do not contribute to the photogeneration process and their absorbed energies will produce phonons that convert to heat. Photons with energy above the bandgap energy will generate a photocurrent. The remaining energy above the bandgap will convert to kinetic energy that will also generate heat. This heat have a negative effects on the solar cell's performance.

An increase in the solar cell temperature will cause a decrease in the bandgap energy, which will allow more photons to be absorbed. This increase in absorption will slightly increase the short-circuit current. Furthermore, a rise in the solar cell's temperature will have a negative impact on the open-circuit voltage and the fill factor which will eventually reduce the cell's efficiency. Ref [6] reports that the output power of Si PV cell decreases 0.47%/°C.

Experimental measurements of temperature effects on crystalline silicon solar cell showed that with increased operating temperature, a decrease of 0.65%/K in the PV cell

output power, a fill factor decrease of 0.2%/K, and a conversion efficiency decrease of 0.08%/K [7].

Solar cells can undergo long-term degradation if operating temperature exceeds certain limits [8]. The temperature degradation coefficient is usually given by the solar cell's manufacturer along with its maximum operating temperature. It is important to control the solar cell's temperature by removing of excess heat. Different techniques of cooling solar cells have been introduced, and we will explore them in the next section.

1.4 Thermal Managements of Solar Cells

Only a fraction of absorbed solar radiation energy is turned into useful output. The rest is converted to heat inside the cell. This heat is removed by two main approaches, passive cooling and active cooling [9].

1.4.1 Passive cooling

Passive cooling is the removal of heat by flowing medium like air or water. Most solar cells uses passive cooling because of its reliability and low cost. Examples of passive cooling include heat sinks, heat pipes, and microchannels.

A heat sink is a metal device that absorbs the heat from the solar cell and dissipates it into the surrounding air by natural or forced heat convection [4]. Heat sinks are made of materials with high thermal conductivity like aluminum or copper. They can be shaped as a flat panel below a solar cells array with fin arrays in one side, or many sides if the design allows or using single solar cell. Natural conviction occurs when cooling air flows normally

through the fin array, whereas forced conviction is when air flow is forced by the use of a fan. Forced cooling provides a more cooling than natural cooling but requires additional power to operate the fan. Natural cooling is preferred for solar cells as it is easier to implement and cost less. Heat sinks are optimized by changing the geometrical shape of the fins. Water can also be used to cool heat sinks. In this case, more heat exchange takes place due to the higher heat capacity of water [9]. Output power of a forced air cooling PV cell increased by 10% over natural air cooling and 66% with water cooling [10].

Heat pipes are another method of passively cooling solar cells [11]. Heat pipes are metal pipes filled with small amount of water that transfers heat by evaporating and condensing in continuous cycles. They require no input power and can effectively transfer heat over a long distance. When heat is absorbed at one end of the pipe, it causes water to evaporate. The increasing vapor pressure results in a difference in pressure which drives the vapor to the other end of the heat pipe, the condenser section, which is placed in a cooler environment. The section between the hot and cold ends is the transfer section where two states of the liquid flow in opposite directions. Heat pipe cooling is a suitable option for solar cells under concentrated conditions due to its excellent thermal conductivity and constant temperature uniformity. Fins can be utilized at the condenser section to increase heat exchange.

Microchannel cooling is another form of passive cooling that can transfer large amount of heat from a small area. A rectangular channel made of high thermal conductivity material where inner fluid thermal conductivity is inversely proportional to the channel width.

1.4.2 Active cooling

Active cooling is done by collecting heat from the solar cell and using it in other useful applications such as water heating. This technique is also referred to as photovoltaic/thermal collector, PV/T, and it utilizes both electrical and heat energies of the system.

1.5 Thermal Interface Materials

Thermal interface materials (TIMs) are used to enhance the thermal conductance between two contacting surfaces [2, 12-14]. When two adjoining surfaces such as the solar cell back panel and a heat panel are joined together to transfer heat, air gaps caused by defects in the two surfaces can cause thermal contact resistance between the two surfaces. Thermal interface materials, generally in the form of paste, is used to fill these air gaps and provide a better thermal contact between the two surfaces.

Thermal interface material performance depends on its thermal conductivity. The higher thermal conductivity for the TIM the better thermal contact between the two surfaces. While TIMs provide better thermal conductance than air, they are less heat conducting than heat conducting metals like aluminum or copper. TIMs are made of composite materials with metallic or ceramic fillers that enhances thermal conductivity. Solid metallic particles like aluminum or silver provide a better thermal conductance and when ceramic particles are used when electrical insulation is required.

Thermal interface materials must also be designed to spread effectively under surfaces pressure. A TIM that has a better spreading characteristics can enhance the interfacial thermal contact by eliminating more air pockets between the two surfaces.

Another important feature to consider in choosing thermal interface materials is its durability. Performance stability and reliability of TIMs over long operating times is important and TIMs with higher viscosities are used for this.

It is crucial to apply TIMs appropriately. Excess amounts can have negative results and amounts that are too low can result smaller spreading than required. The TIM must also be easily removed when replacement is required.

Other factors to consider in TIMs include cost and corrosion resistance. Fillers made from silver or graphene provides excellent thermal conductivities but cost much more that other fillers like aluminum. Additionally, TIMs must not cause long time corrosions to surfaces where they’re applied.

A typical use of thermal interface material (TIM) can be seen in figure 1-2 where it is applied between two surfaces, the back surface of a heat generating source, a solar cell in this case, and the surface of a heat sink or heat spreader. A zoomed in view of the surfaces contacts reveals the microscopic surfaces imperfections caused by the surfaces roughness and the air gaps that are filled with the interface material.

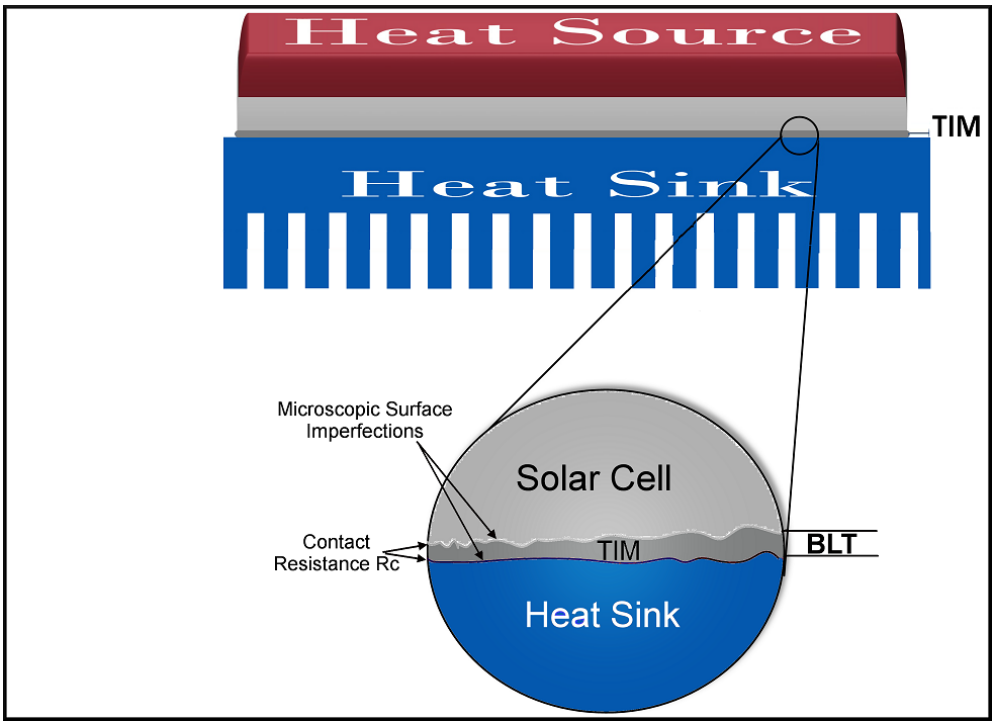

Figure 1.2: Thermal interface material used to fill the gaps between the two surfaces.

The distance between the two surfaces is called the bond-line thickness (BLT) and the contact resistances between TIM and the two surfaces, R_{C1} and R_{C2}, are used to calculate the TIM effective thermal resistance, R_{TIM}:

$$R_{TIM} = \frac{BLT}{K_{TIM}} + R_{C1} + R_{C2}$$

Where K_{TIM} is the thermal conductivity of the TIM [2].

1.6 Graphene

Graphene is a sheet of single-layered carbon atoms packed densely into a honeycomb crystal lattice[2]. Prior to its discovery in 2004, suspended graphene was not considered to exist in a free state [15]. Graphene is characterized by its high intrinsic thermal conductivity

ranging from 3-5.3 KW/m K, high electron mobility, and low resistivity [16-18]. The superior thermal and electrical properties of graphene make it an excellent material for thermal management, low noise transistors, and electrical interconnects [16].

1.6.1 Graphene to Improve Thermal Conductivity of TIM

The ongoing decrease in electronics size and increase in its power density have raised the demand for better thermal management and heat dissipation [19]. The development of an improved thermal interface material with higher thermal dissipation crucial to the thermal management of next generation electronics [2]. Conventional TIMs are generally made of polymeric or grease base material loaded with conductive materials like silver particles at high loading volume fractions f reaching up to 70% [19, 20]. The increase in loading fraction f can negatively affect the TIM performance and increase its cost. Several attempts have been made to develop a hybrid graphene-metal based thermal interface materials with a reduced loading fraction f [13, 19-21]. A report of 500% increase in thermal conductivity of the TIM was observed with the addition of small graphene volume loading fraction of $f \sim 5\%$ [19]. This significant improvement in the TIM thermal conductivity is largely owed by the superb intrinsic thermal conductivity of graphene and the strong graphene coupling to matrix materials [19].

Chapter 2

Experiment Setup

This chapter describes the devices used and processes of using them to get our final results.

2.1 Equipment Used

In these experiments we have used the following devices:

Solar cells simulation module which consists of a 600W high pressure sodium bulb that produces light intensity of 85,000 lumens and 2,100 K color temperature, two solar cells each with a heat sinks attached to it. The heat sinks are screwed to the solar cells where the solar cells are inside the enclosure and the heat sinks are outside. Between them is the enclosure chassis with an opening so that the solar cell's back is touching the heat sink. This is where the thermal interface material is applied.

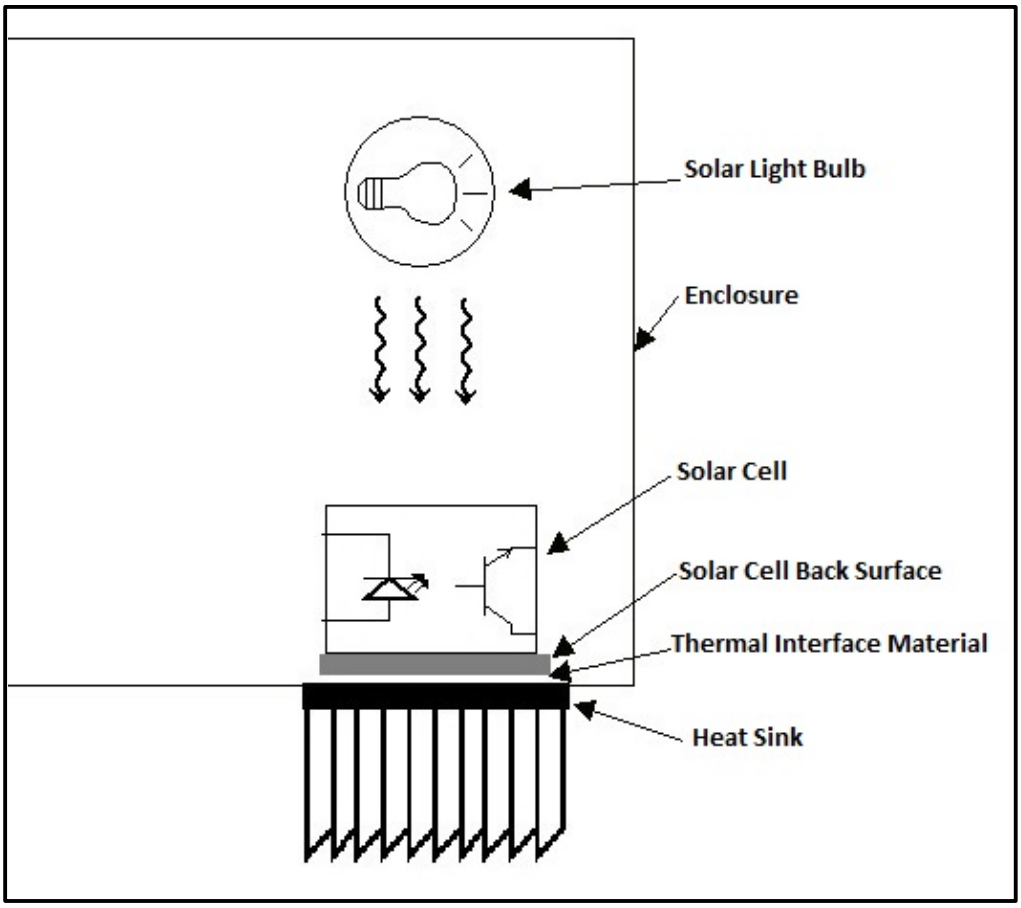

Figure 2.1: Schematic of the solar cells module

A precision electronic weight balance is used to measure the thermal interface materials and graphene to be mixed [22].

A magnetic stirrer is used to mix the thermal paste with the graphene nano-powder.

A power screw driver with adjustable torque settings. This device insures that we have the same torque setting when securing the solar cell to the heat sink in all test trials. This subsequently provides a uniform pressure for the thermal interface material.

A multi-channel temperature logger is used to log the heat sink and ambient temperatures every 10 seconds [23].

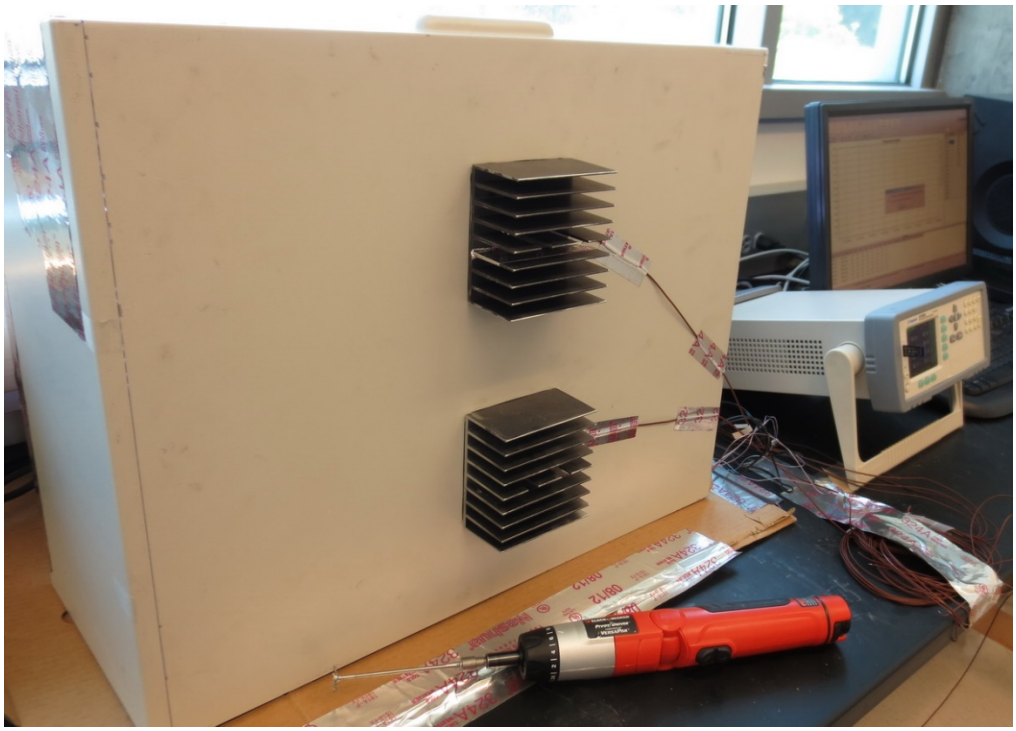

Figure 2.2: Image of the solar cells testing module.

2.2 Materials used

Three commercial thermal interface materials were used [24-26]. Their properties are listed in table 2.1

Table 2.1: Physical properties of top commercial thermal interface materials.

TIM	Filler Material	Density (g/cm^3)	Cure Time (Hrs.)
MX-4	Carbon	2.5	N/A
Arctic Alumina	Aluminum oxide	1.6	50-200
Arctic Silver 5	Silver, Aluminum oxide	4.1	50-200

Graphene nanopowder with average flake thickness of 12 nm, Figure 2.3. The dry powder has a 99.2% purity and 2.25 g/cm^3 density.

Figure 2.3: 12 nm graphene nanopowder

Ethyl alcohol is used to ease the mixing process.

2.3 Experimental Procedure

The basic steps of the TIMs mixing and testing process is outline in figure 2.4. The thermal interface materials was weighed by the precision electronic balance and added to a beaker. The weight measurements were noted to the milligram precision. After that, a small amount of 12 nanometer graphene nanopowder was added to the paste in accordance with the following weight percentage formula:

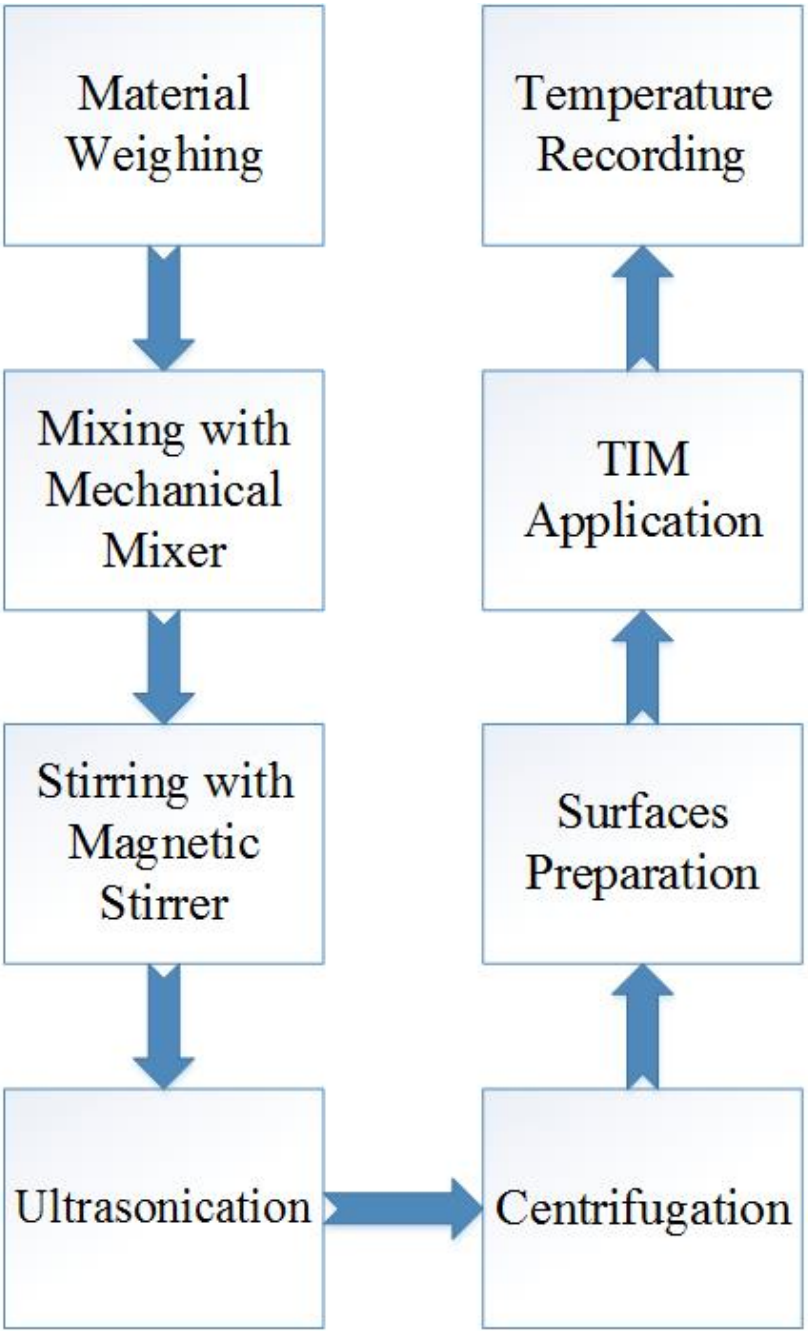

Figure 2.4: Basic steps of TIMs mixing and testing

$$Graphene\ wt\% = \frac{Graphene\ Weight}{TIM\ Weight + Graphene\ Weight}$$

And we convert the weight fraction to volume fraction using:

$$Graphene\ Vol\% = \frac{Graphene\ Weight}{Graphene\ Density} \div \left(\frac{Graphene\ Weight}{Graphene\ Density} + \frac{TIM\ Weight}{TIM\ Density}\right)$$

Table 2.2 shows the different types and weights of thermal interface materials and phase change material used, the graphene weight and calculated weight fraction and volume fraction.

Table 2.2: Weights of thermal interface materials and graphene that were mixed together along with graphene wt% and %vol.

TIM Type	TIM Weight (mg)	Graphene Weight (mg)	MLG Wt%	MLG Vol%
Arctic Alumina	1026.9	10.8	1.04%	0.74%
Arctic Alumina	5506	109.7	1.95%	1.4%
Arctic Alumina	5381	168.8	3.04%	2.18%
Arctic MX-4	1995.8	19.2	0.95%	1.06%
Arctic MX-4	2291.8	50.1	2.14%	2.37%
Arctic MX-4	831.2	25.9	3.02%	3.35%
Arctic Silver 5	4723	48.7	1.02%	1.84%
Arctic Silver 5	2214.5	48.2	2.13%	3.81%
Arctic Silver 5	2541.2	76.54	2.92%	5.2%

The compound is then mixed carefully with the addition of ethyl alcohol to aid in the mixing process. Using a mechanical mixer, the compound is mixed continuously for about 1 hour. After that, a magnetic stirrer is used to mix the compound for 3-4 hours or until most of the ethyl alcohol has evaporated. The compound is then allowed to rest for about 30 minutes.

Before applying the mixed compound, both the surfaces of the solar cell and heat sinks were prepared and cleaned using special solutions of thermal material removing and a thermal surface purifying. This step insures no TIM residual remains on the surface and interferes with the current TIM tested.

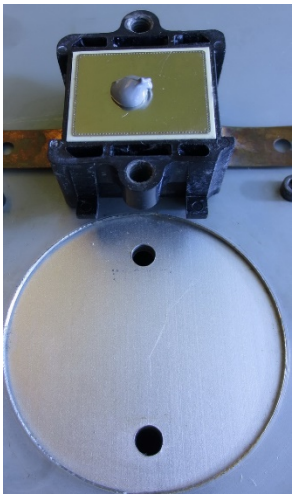

Figure 2.5: Application of thermal interface material

After surfaces preparation, the mixed compound is applied in to the solar cell thermal back surface as shown in figure 2.5. Both surfaces were then secured together by two screws. The screws were tightened to a standard torque using power screw driver. This step is to insure a uniform pressure throughout all tests.

Manufacturer's recommended cure times for every TIM were observed and several thermal cycling were employed to reach optimal settings.

Using multi-channel temperature logger, the heat sinks and ambient temperatures were recorded every 10 seconds with a time and date stamp. Table 2.3 shows a sample of recorded date where two thermocouples are used to record the ambient temperature and

two for the two heat sinks. The ambient temperature used for calculations is the average between the two recordings.

Table 2.3: Sample of recorded temperature values

Date/Time	Ambient 1	Heat Sink 1	Heat Sink 2	Ambient 2
5/1/2013 18:46	22.8	41.7	43	22.4
5/1/2013 18:46	22.8	41.8	43	22.5
5/1/2013 18:46	22.7	41.9	43	22.4
5/1/2013 18:47	22.7	41.9	43	22.4
5/1/2013 18:47	22.7	41.8	42.9	22.4
5/1/2013 18:47	22.7	41.8	42.9	22.4
5/1/2013 18:47	22.5	41.3	42.4	22.3

The difference between heat sink temperature and ambient temperature (ΔT) is measured and averaged over a period of one hour. Since we're reading the temperature from the heat sink, it follows that the TIM with higher thermal conductivity would result in a higher ΔT. Similarly, the less thermal conductivity of TIM the lower ΔT will be.

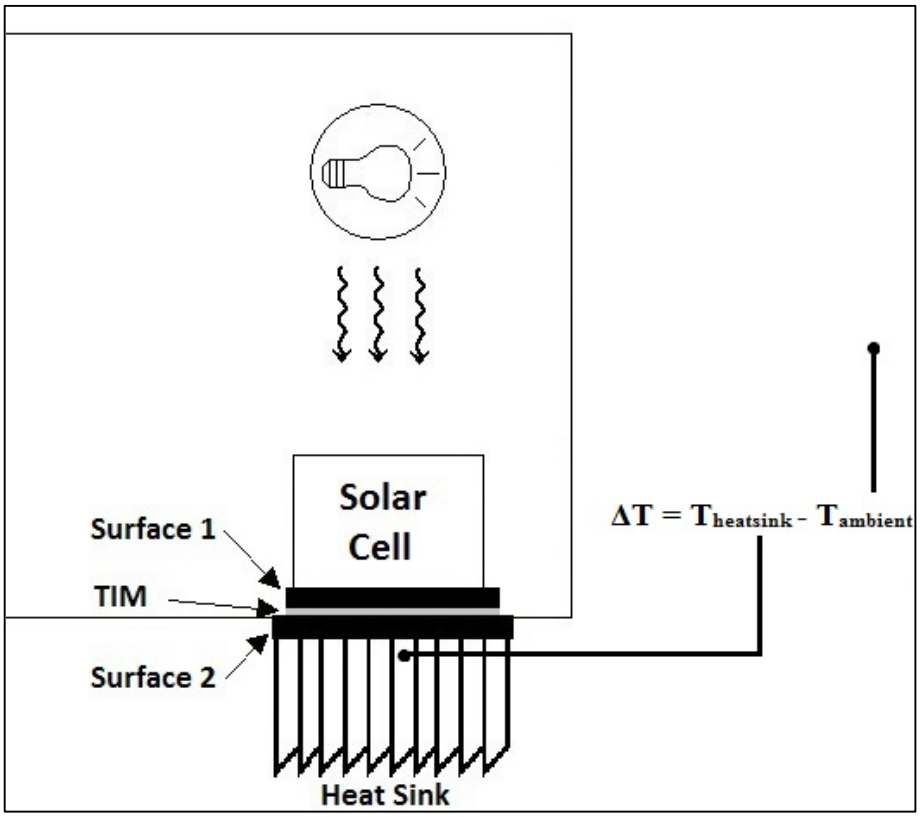

Figure 2.6: Measurements of ΔT

If a thermocouple probe is placed on the solar cell inside the enclosure, the radiation energy from the solar cell light can heat the probe and affect the reliability of the results. For this reason, we used the alternative method described above to evaluate thermal conduction.

Because every solar cell has its unique surface defects and exposure to light, we have used the same solar cell for all thermal interface materials mixed. For example, all Arctic Silver Arctic Alumina mixtures were all tested on the same solar cell.

2.4 Spreading Characteristics of TIM

Different TIM pastes have different spreading characteristics. When applying TIM and joining the two surfaces, it is important that the TIM spreads under applied pressure to cover the entire contacting area between the two surfaces. A typical spreading behavior can be seen in figure 2.7 where the TIM has covered the entire surface.

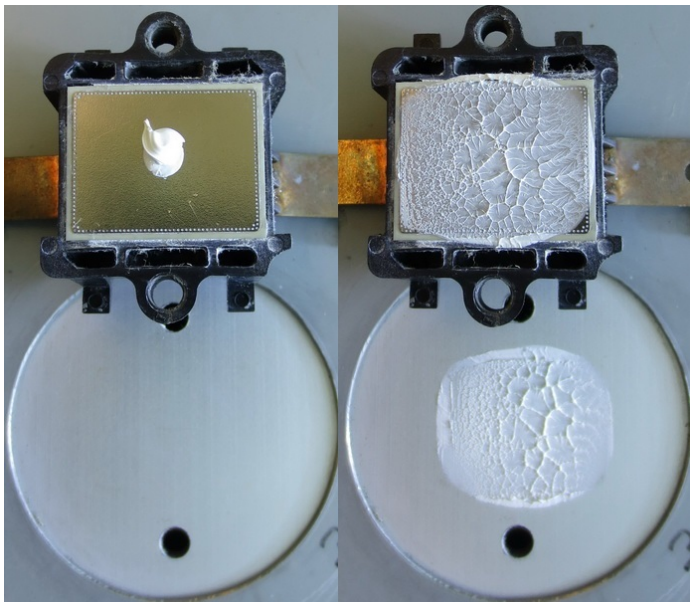

Figure 2.7: Typical spreading of thermal interface material

Using insufficient amount of TIM can results in spreading similar to the one shown in figure 2.8 where the TIM has not spread to cover the entire surface and the remaining uncovered portion can cause an increase in the thermal resistance.

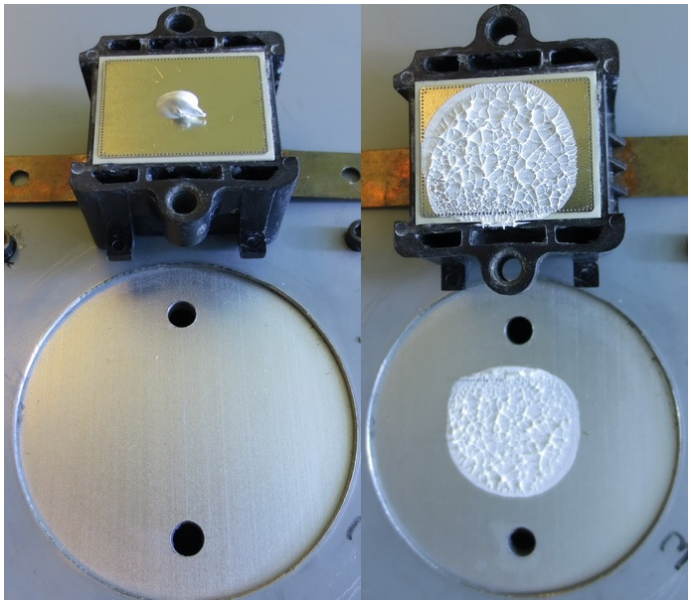

Figure 2.8: Insufficient use of TIM causing poor spreading of thermal interface material

On the other hand, using excessive amount of TIM can increase the bond-line thickness, BLT, of the TIM and result in an increase in the overall thermal resistance figure 2.9.

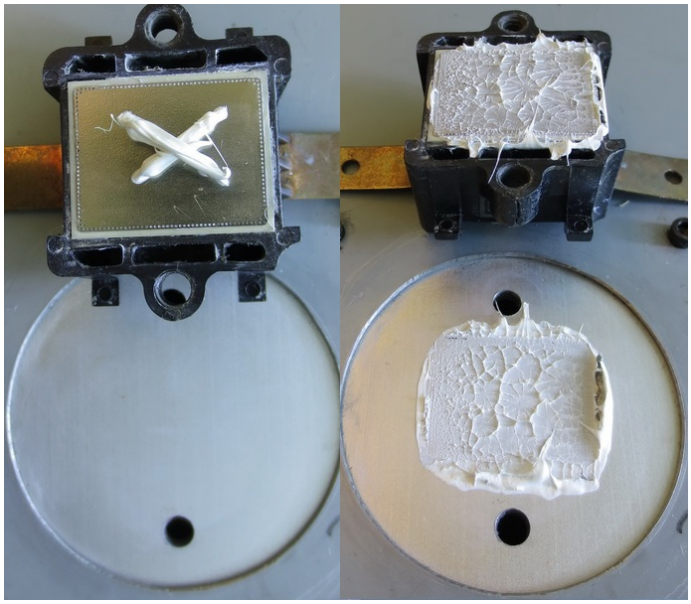

Figure 2.9: Excessive use of thermal interface material can increase the bond-line thickness BLT.

The way TIM spreads is also affected by the density and viscosity of the TIM. Figure 2.10 shows the poor spreading of a TIM due to its high density and low viscosity. In such case, a manual spreading of the TIM is required where a thin layer of the paste is evenly spread over the surface as shown in figure 2.11.

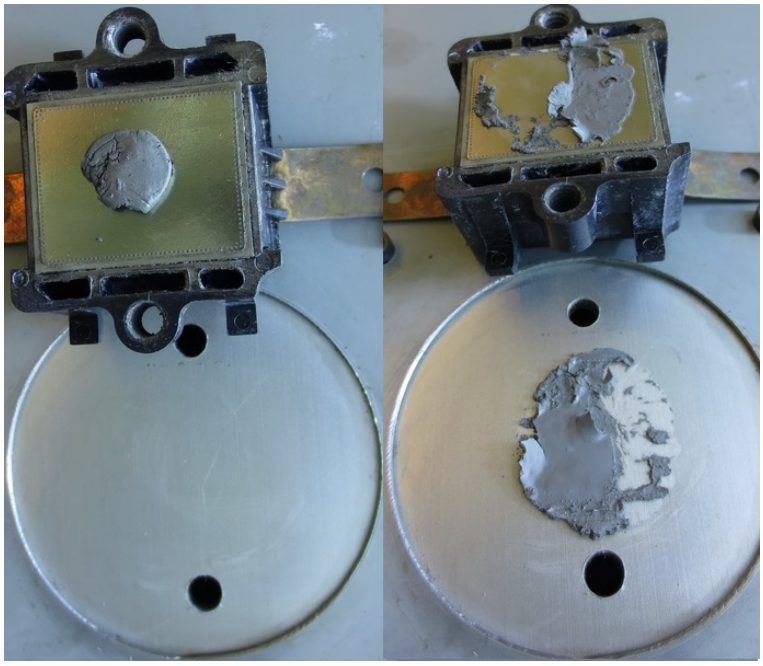

Figure 2.10: Weak spreading of thermal interface material caused by the high density and low viscosity of the compound.

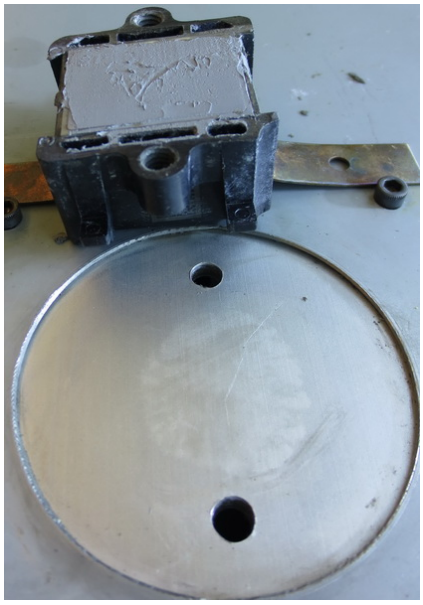

Figure 2.11: Manual spreading of thermal interface material

2.5 Validity and Reliability of Data

Great care has been undertaken to insure the accuracy of measurements and similarity of test trials. However, there are some limitation factors that must be addressed like device's accuracy and surface's degradations.

One important factor that changes with every trial is the TIM application method. No two trials have the exact same TIM spreading due to changes in the TIM viscosity with each addition of dry graphene powder.

Another factor is the degradation of the solar cell and heat sink's surfaces with use over time. More scratches and surface defects are introduced to both surfaces which results in a change in the measured data. Figure 2.12 shows the surface scratches developed from continuous usage.

Figure 2.12: Developed Surface defects arising from continuous use

Chapter 3

Results and Inference

3.1 Results

Several commercial TIMs loaded with 1-3 wt% graphene were tested between interfaces of solar cell and heat sink. Their thermal conductance was evaluated as a function of ΔT, the difference between heat sink and ambient temperatures. Temperature values were taken after observing recommended TIM cure times and thermal cycling. TIMs with higher thermal conductivity transfer more heat from the solar cell to the heat sink, which then leads to an increase in the heat sink temperature. The change in ambient temperature over time and between test trials causes a change in the internal temperature of the testing module. Therefore, the ambient temperature is subtracted from the heat sink temperature to account for this change.

3.1.1 Arctic MX-4

Figure 3.1 compares ΔT for Arctic MX-4 at different graphene wt% loading (0%-3%) over time. The 0% line represents the reference value of the TIM with no graphene being added to it.

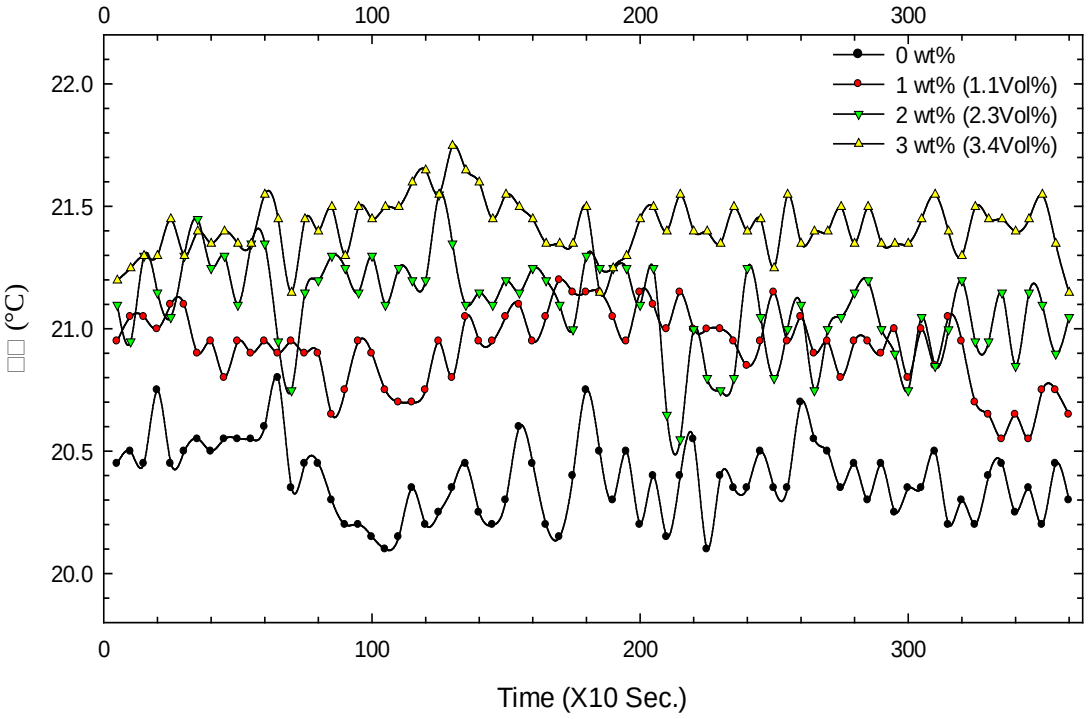

Figure 3.1: ΔT over time for Arctic MX-4 mixed with 0-3 wt% graphene.

For the sake of comparison, and despite the Arctic MX-4 manufacturer indication of no cure time is requirement, the results were taken after curing time that matches that of the other two TIMs.

By averaging the individual ΔT measurement for each of the four compounds tests (0-3 wt%) over an hour, we can see that ΔT increase with increasing graphene weight fraction as shown in table 3.1.

Table 3.1: average and percentage increase of ΔT for Arctic MX-4 with (0-3) graphene wt%.

Graphene wt%	Average ΔT (°C)	ΔT Increase (%)
0%	20.38	0%
1%	20.92	2.65%
2%	21.1	3.53%
3%	21.4	5.01%

The increase of ΔT as a function of graphene weight fraction for Arctic MX-4 is illustrated in figure 3.2. The increase in ΔT as a result of using more graphene weight fraction is evident. From this we conclude that the performance of Arctic MX-4 TIM is enhanced when adding graphene powder as filler.

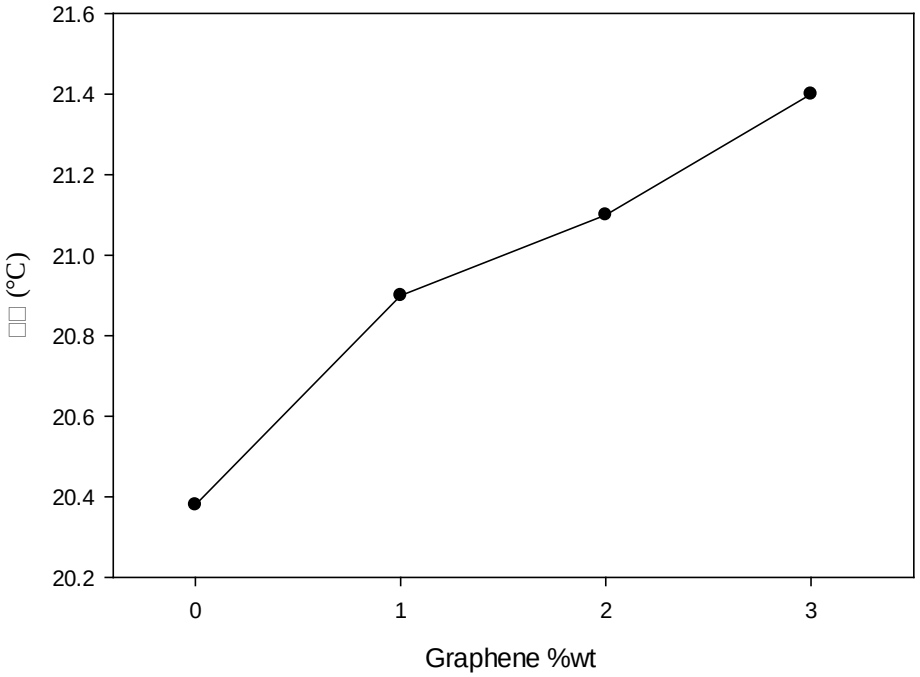

Figure 3.2: : ΔT as a function of graphene weight fraction for Arctic MX-4.

3.1.2 Arctic Alumina

Figure 3.3 illustrates ΔT as a function of time resulting from the four Arctic Alumina compounds tested at graphene weight fraction from 0%-3%. The performance of this TIM improved more significantly when using graphene as a filler, with 12.1% increase in ΔT when using 3% graphene weight fraction compared to no graphene usage.

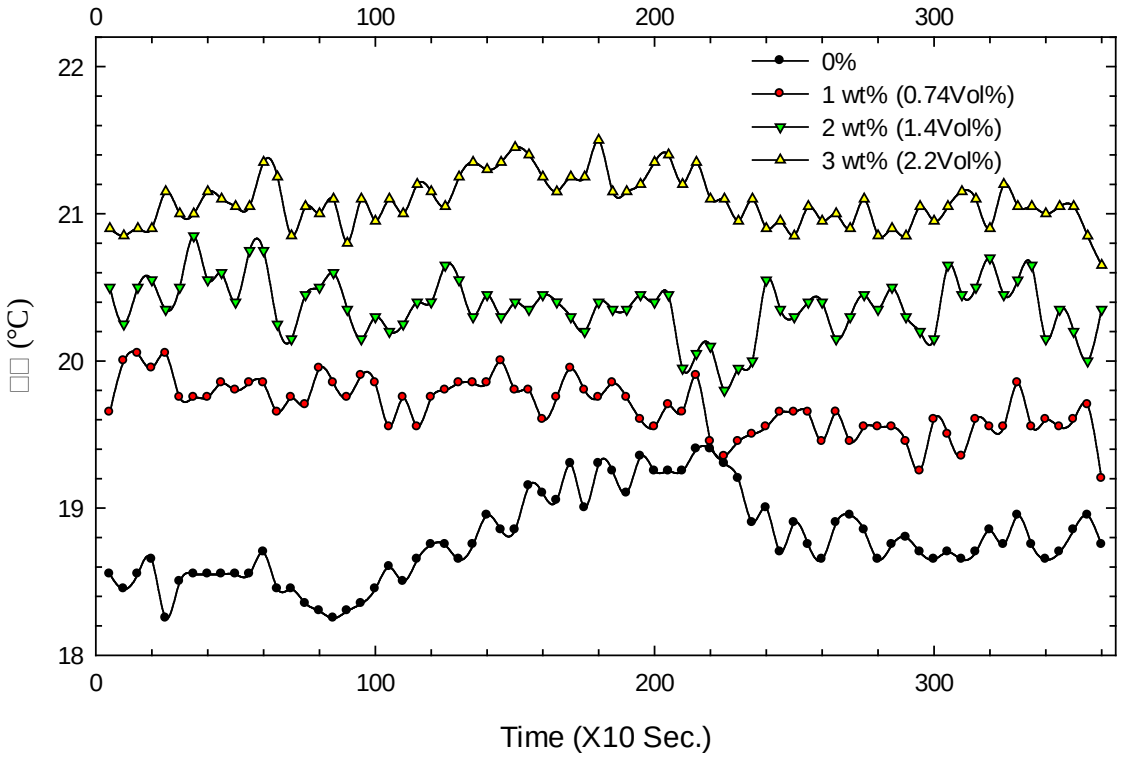

Figure 3.3: ΔT over time-for Arctic Alumina mixed with 0-3 wt% graphene.

The averaged ΔT for the four trials of Arctic Alumina are listed in table 3.2.

Table 3.2: average and percentage increase of ΔT for Arctic Alumina with (0-3) graphene wt%.

Graphene wt%	Average ΔT (°C)	ΔT Increase Percentage
0%	18.79	0%
1%	19.69	4.8%
2%	20.38	8.5%
3%	21.07	12.1%

Figure 3.4 shows ΔT as a function of graphene weight fraction for Arctic Alumina. A steady and more visible increase in ΔT with each additional graphene weight fraction can be seen.

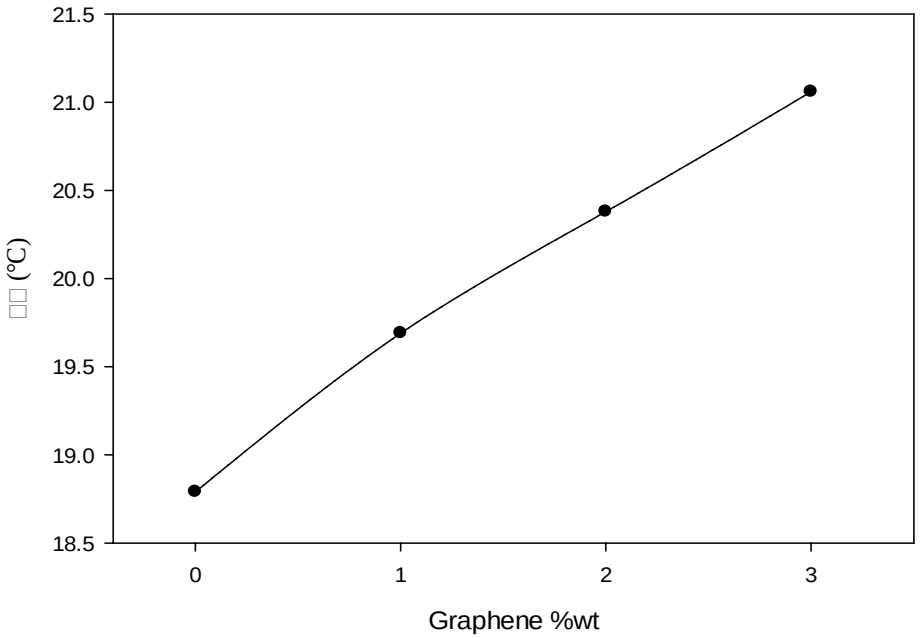

Figure 3.4: ΔT as a function of graphene weight fraction for Arctic Alumina.

3.1.3 Arctic Silver 5

The measured ΔT for the four Arctic Silver 5 compounds can be seen in figure 3.5. This TIM exhibits less performance change with each increase in graphene wt%. Only an increase of 2.44% in ΔT is resulted from adding 3% weight fraction of graphene.

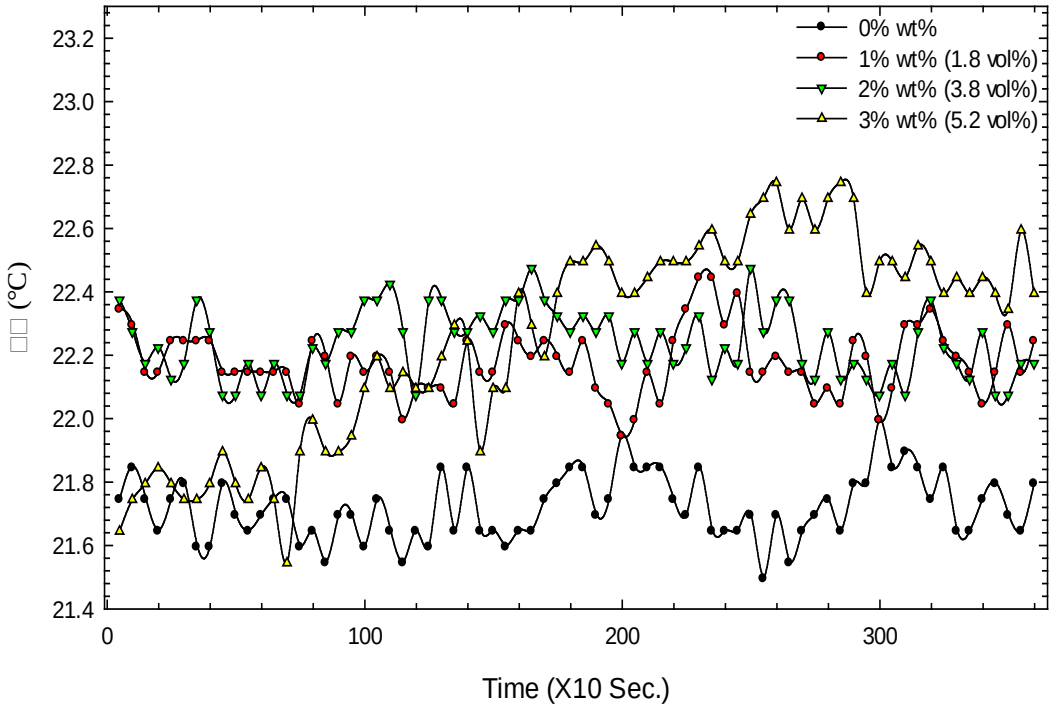

Figure 3.5: ΔT over time-for Arctic Silver 5 mixed with 0-3 wt% graphene.

Table 3.3 shows the average and percent increase of ΔT for the four trials of Arctic Silver 5.

Table 3.3: average and percentage increase of ΔT for Arctic Silver 5 with (0-3) graphene wt%.

Graphene wt%	Average ΔT (°C)	ΔT Increase Percentage
0%	21.72	0%
1%	22.18	2.12%
2%	22.23	2.35%
3%	22.25	2.44%

Figure 3.6 shows ΔT increasing as a function of graphene weight fraction used.

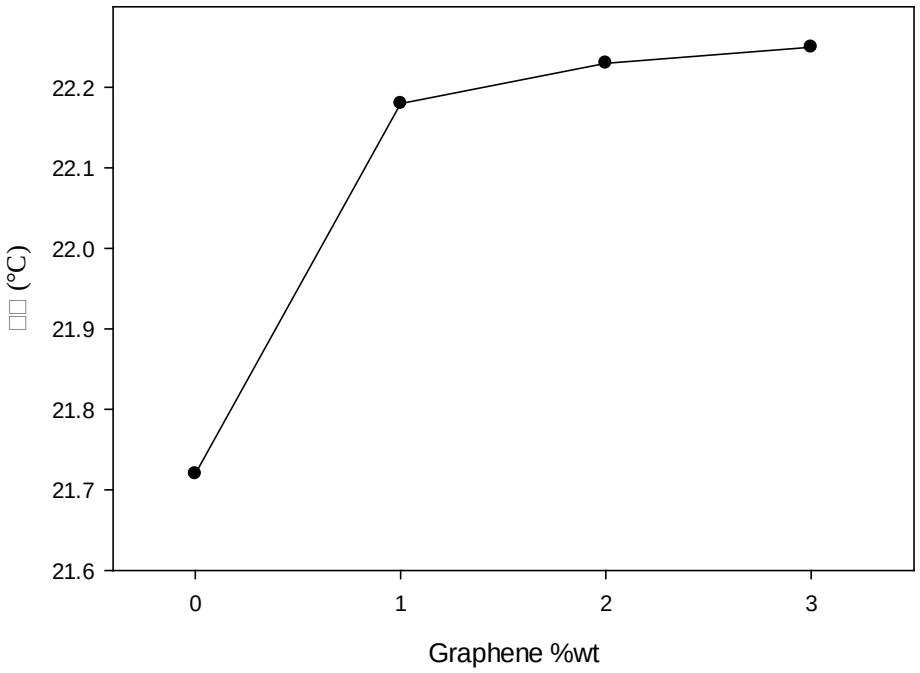

Figure 3.6: ΔT as a function of graphene weight fraction for Arctic Silver 5.

3.2 Discussion

Thermal interface materials aim at reducing the thermal resistance between two adjoining surfaces R_{TIM}. This resistance is affected by several factors like the TIM thermal conductivity K_{TIM}, thermal contact resistances between the TIM and the two surfaces R_c, and the distance between the two surfaces or bond-line thickness BLT. These factors are related to R_{TIM} by the following equation:

$$R_{TIM} = \frac{BLT}{K_{TIM}} + R_{C1} + R_{C2}$$

The thermal conductivity of the TIM is affected by the filler volume fraction, the thermal conductivity of the matrix and filler, and the contact resistance between the fillers and matrix. The contact resistance between the matrix and filler can increase due to improper mixing of the filler and polymer matrix.

Table 3.4 lists the physical characteristics of the three TIMs used in our study. The filler particles already existing in the base TIM, density, ΔT increase at 3 wt% of graphene, and coverage. The coverage of the base TIM is a measurement of the area in cm^2 that one gram can cover at layer thickness of 0.075 mm.

Table 3.4: Physical characteristics of the three TIMs and incrase percentage of ΔT when loaded with 3 wt% of graphene

TIM	ρ (g/cm^3)	Filler	Coverage	ΔT
MX-4	2.5	Carbon	63	5.1%
Alumina	1.6	Al_2O_3, BN,	88	12%
Silver 5	4.1	Ag, ZnO, Al_2O_3, BN	30	2.44%

Arctic Silver 5 base TIM consists of 88% filler weight fraction. TIMs with high filler loading fractions generally causes an increase of BLT and K_{TIM}. With the addition of MLG the filler weight fraction was increased further and the mixed compound had a weaker spreading characteristics. It is reasonable to assume that this was the limiting factor that caused the low change in ΔT.

On the other hand, the less dense and more viscous Arctic Alumina had relatively better spreading characteristics when mixed with MLG powder. With these physical differences, we were able to obtain a better and more consistent improvement of ΔT when mixing MLG with Arctic Alumina as opposed to the declining ΔT improvement with Arctic Silver 5. Figure 3.7 compares ΔT improvement as a function of graphene wt% for the three TIMs.

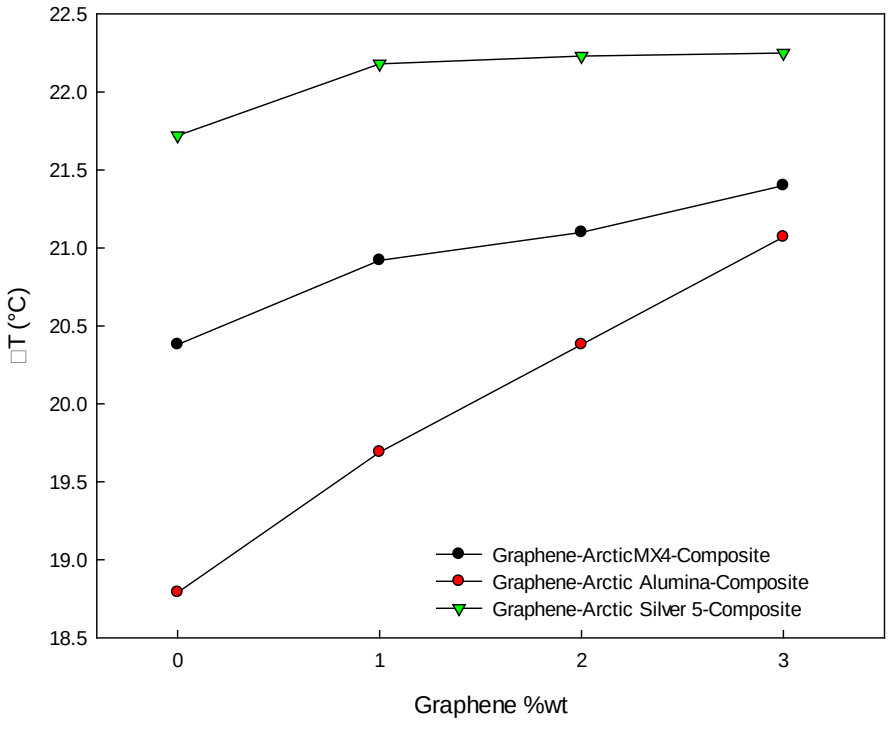

Figure 3.7: ΔT as a function of graphene weight fraction for the three tested TIMs

3.3 Conclusion

This thesis presented the results of experimental approaches to improve thermal interface conductance between solar cells and heat spreaders by developing better thermal interface materials. Three major commercial TIMs were mixed with multi-layer graphene nanopowder at different weight fractions and tested a solar cell module. The performance of the three TIMs were improved with the graphene addition. Physical properties of the base TIMs, like density, viscosity, and filler loading fractions were factors in determining the level of performance increase of the hybrid MLG-TIM compounds. TIMs that have lower density, less volume loading fraction, and higher viscosity gave better and steadier thermal performance when mixed with graphene.

References

[1] F. Sohrabi, A. Nikniazi, and H. Movla, Optimization of Third Generation Nanostructured Silicon- Based Solar Cells, 2013.

[2] X. C. Tong, Springer Series In Advanced Microelectronics: Advanced Materials for Thermal Management of Electronic Packaging: Springer New York, 2011.

[3] H. S. Nalwa, Encyclopedia of Nanoscience and Nanotechnology: American Scientific Publishers, 2004.

[4] "Thermal design; heat sinks, thermoelectrics, heat pipes, compact heat exchangers, and solar cells," Sci-Tech News, vol. 65, pp. 35-35, 2011.

[5] C. J. Chen, Physics of Solar Energy: Wiley, 2011.

[6] M. Roger, G. Yogi, U. Hari, R. Takhir, T. Ayodhya, W. Roland, et al., "Photovoltaics Fundamentals, Technology and Application," in Handbook of Energy Efficiency and Renewable Energy, ed: CRC Press, 2007, pp. 23-1-23-63.

[7] E. Radziemska, "The effect of temperature on the power drop in crystalline silicon solar cells," Renewable Energy, vol. 28, pp. 1-12, 1// 2003.

[8] A. Royne, C. Dey, and D. Mills, "Cooling of photovoltaic cells under concentrated illumination: a critical review," Solar Energy Materials and Solar Cells, vol. 86, pp. 451-483, 2005.

[9] Z. Ye, Q. Li, Q. Zhu, and W. Pan, "The cooling technology of solar cells under concentrated system," in Power Electronics and Motion Control Conference, 2009. IPEMC '09. IEEE 6th International, 2009, pp. 2193-2197.

[10] S. Bojanampati, P. Rodgers, and V. Eveloy, "Experimental assessment of flat-type photovoltaic module thermal behavior," in Thermal, Mechanical and Multi-Physics Simulation and Experiments in Microelectronics and Microsystems (EuroSimE), 2012 13th International Conference on, 2012, pp. 1/4-4/4.

[11] M. A. Farahat, "Improvement the thermal electric performance of a photovoltaic cells by cooling and concentration techniques," in Universities Power Engineering Conference, 2004. UPEC 2004. 39th International, 2004, pp. 623-628 vol. 1.

[12] R. Khandelwal and J. M. C. Kishen, "Thermal weight functions for bi-material interface crack system using energy principles," International Journal of Solids and Structures, vol. 45, pp. 6157-6176, Dec 1 2008.

[13] M. O. Memon, S. Haillot, and K. Lafdi, "Carbon nanofiber based buckypaper used as a thermal interface material," Carbon, vol. 49, pp. 3820-3828, Oct 2011.

[14] X. B. Li and R. G. Yang, "Effect of lattice mismatch on phonon transmission and interface thermal conductance across dissimilar material interfaces," Physical Review B, vol. 86, Aug 27 2012.

[15] K. S. Novoselov, A. K. Geim, S. V. Morozov, D. Jiang, Y. Zhang, S. V. Dubonos, et al., "Electric Field Effect in Atomically Thin Carbon Films," Science, vol. 306, pp. 666-669, October 22, 2004 2004.

[16] A. A. Balandin, S. Ghosh, W. Bao, I. Calizo, D. Teweldebrhan, F. Miao, et al., "Superior Thermal Conductivity of Single-Layer Graphene," Nano Letters, vol. 8, pp. 902-907, 2008/03/01 2008.

[17] D. Konatham, D. V. Papavassiliou, and A. Striolo, "Thermal boundary resistance at the graphene-graphene interface estimated by molecular dynamics simulations," Chemical Physics Letters, vol. 527, pp. 47-50, Feb 27 2012.

[18] A. Alofi and G. P. Srivastava, "Thermal conductivity of graphene and graphite," Physical Review B, vol. 87, Mar 18 2013.

[19] V. Goyal and A. A. Balandin, "Thermal properties of the hybrid graphene-metal nano-micro-composites: Applications in thermal interface materials," Applied Physics Letters, vol. 100, Feb 13 2012.

[20] K. M. F. Shahil and A. A. Balandin, "Thermal properties of graphene and multilayer graphene: Applications in thermal interface materials," Solid State Communications, vol. 152, pp. 1331-1340, Aug 2012.

[21] K. M. F. Shahil and A. A. Balandin, "Graphene-Multilayer Graphene Nanocomposites as Highly Efficient Thermal Interface Materials," Nano Letters, vol. 12, pp. 861-867, Feb 2012.

[22] I. A&D ENGINEERING, "HR-60 analytical balance Manual," p. 40, 2013.

[23] I. Applent Instruments, "AT4516 Multi-Channel Temperature Meter " p. 5, 2011.

[24] I. Arctic Silver, "Arctic Silver 5 MSDS," p. 2, August 23, 2012 2012.

[25] I. Arctic Silver, "Arctic Alumina MSDS," p. 2, August 23, 2012 2012.

[26] A. AG, "ARCTIC MX-4 Spec Sheet," p. 2, 2011-03-03 2013.